

Variational Treatment of a Vibrating LiNbO_3 -Based Rectangular Hybrid Structure: the Developing of a Functional for Computing Surface-Load Configurations

Oleksiy I. POLOVINA, Vasyl V. KURYLIUK, Oleg A. KOROTCHENKOV

Kiev National University, Department of Physics
Kiev 03680, Ukraine
e-mail: polovina@univ.kiev.ua

(received February 20, 2007; accepted January 29, 2009)

Electrically-excited electroelastic extensional vibrations of an arbitrarily cut three-dimensional piezocrystal resonator are analyzed variationally. A set of trigonometric trial functions applicable to a waveguide behavior of the resonator partly covered by metal electrodes is proposed. The dependence of the content of the vibration modes sustained by the resonator on the electrode configuration is found. The frequency spectra taken in 128° - Y -rotated LiNbO_3 rectangular plates exhibit a good conformity with the computed resonator eigenfrequencies.

Keywords: electroelastic vibrations, variation computations, hybrid structures, eigenfrequencies.

1. Introduction

Since the report of ROCKE *et al.* [25] appeared, the dynamical behavior of photoexcited electrons and holes in semiconductor nanostructures modulated by acoustic waves is a topic of increasing interest. The interaction between the free charges and the waves is mostly due to a piezoelectric coupling. In many cases, the size of the acoustoelectric interaction is not large enough because of a weak piezoelectricity of the structures. A greatly enhanced acoustoelectric interaction can be achieved in a hybrid structure which contains a LiNbO_3 plate and a semiconductor nanostructure mounted on it. In these structures, the moving piezoelectric potential of the surface acoustic waves launched in the LiNbO_3 plate and the acoustoelectric interaction between the wave and free charges placed in a close proximity to the plate surface have been extensively addressed both theoretically and experimentally [7]. Piezoelectric fields of Lamb waves in LiNbO_3 plates

has also been reported [6]. Meanwhile, interesting consequences are expected to arise from the interaction of the standing-wave piezoelectric field excited in the LiNbO_3 plate and the two-dimensional electron and hole gases created in the adjacent semiconductor nanostructure.

An important advantage of the rectangular plate geometry for the hybrid structure is the possibility to utilize it in a broad frequency range operating either at standing-wave resonances or at its natural resonant frequencies, thus providing more feasibility in choosing both electrical and elastic field-shapes. Therefore, the major driving force for the study of the piezoelectric-semiconductor structure is the technological importance of the acoustoelectric interaction in the fabrication of nanoelectronic devices. However, one of the limiting restrictions of a broader utilization of these structures is the problem of an accurate theoretical treatment of a vibrating rectangular piezocrystal plate which is partly covered by exciting electrodes.

It is well known that accurate modelling of three-dimensional (3D) electroelastic vibrations can be quite complex in the most general case and requires the application of numerical methods. Variational [12, 14, 32], finite-element [2, 19], and some other [11, 27] approximate methods are therefore widely used. However systematic studies have been done only for piezoceramic circular disks [8, 15, 16, 18, 20]. Several interesting issues related to 3D electroelastic vibrations in rectangular-shaped piezoelectric plates [5, 13], piezoelectric parallelepipeds [12, 21, 22, 29], and piezo-elastic laminates [9, 10, 28] have also been raised. Given that the part of the piezoelectric material boundary covered with electrodes is much less than the uncovered part of the boundary, the transfer function, group delay time, and impedance matrix have been computed for a rectangular piezoceramic plate sustaining the lowest-order symmetrical Lamb-wave by applying the finite-element method [5]. The vibration spectrum of a freely-supported LiNbO_3 parallelepiped plate without any surface load has been addressed by the Rayleigh–Ritz calculation scheme in [22]. The present study develops a new approach to the variational treatment of a 3D LiNbO_3 rectangular-plate resonator by taking into account the waveguide behaviour of a resonator partly covered by electrodes. Furthermore, the electrode configurations providing the excitation of certain vibration modes in the plate are discussed. Although the reported here considerations concern for a thin metal covering of the vibrating plate, it appears attractive to take the results in a broader context. Thus, it appears possible to employ the functional and the trial functions introduced in this work in order to attain the vibration properties of multilayered structures.

2. Formulation of the electroelastic interaction functional

The general variational formulation of electroelasticity in bounded piezoelectric bodies, based on the Hamilton’s variational principle [31], was elaborated

by HOLLAND and EERNISSE [14]. The method involves the Rayleigh–Ritz calculation procedure and has been successfully used for studying vibrations of a piezoceramic parallelepiped with short-circuited electrodes [12] and a two-electroded piezoceramic disk [14].

Figure 1a shows a schematic sketch of the hybrid structure composed of two parallelepiped-shaped piezoelectric layers ($L_X^{(1)} = L_X^{(2)}, L_Z^{(1)} = L_Z^{(2)}$) used in the formulation of the electroelastic interaction functional. Figure 1b displays a model geometry used in this work for numerical computations. The electroelastic vibration of the plate is excited by applying a set of Q_E ac-signals to the Q_E exciting electrodes shown by filled strips in Fig. 1a, where the p -th electrode with an area of $S(p)$ is fed by the signal with the amplitude of $V_G(p)$ and the angular frequency of ω . The plate vibrations are affected by a system of Q_F electrically unloaded, or “free”, electrodes with an area of $\Sigma(q)$ (open strips in Fig. 1a) due to the screening of the piezoelectric fields by the electrodes. The electrical potential $V(q)$ developed on the q -th free electrode is to be determined.

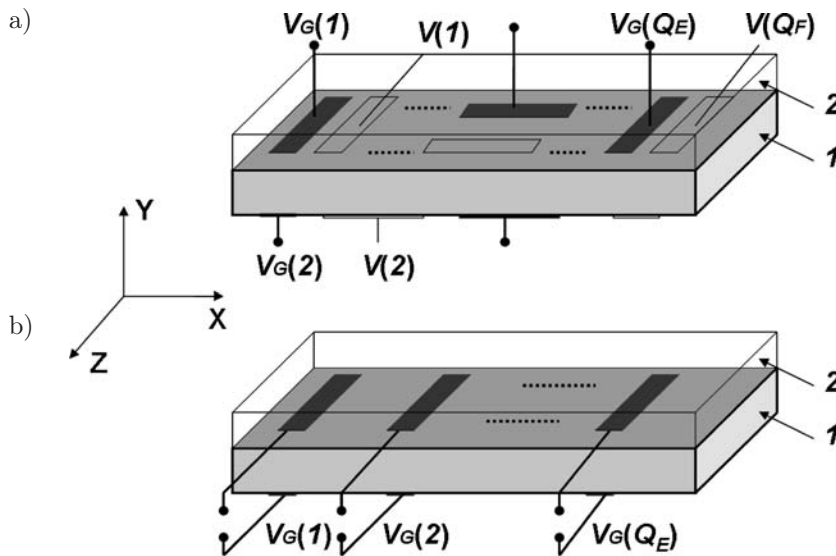


Fig. 1. Schematic sketch of a sample for formulation of the interaction functional (a) and model geometry for numerical computations (b). The sample consists of a LiNbO_3 plate (shaded body) and a set of exciting (filled strips) and free (open strips) electrodes. The total number of exciting and free electrodes are Q_E and Q_F , respectively. They are assumed to be thin enough to cause no mechanical load on the surfaces of the plate. Note the absence of the free electrodes on the surfaces and a bulk excitation of plate vibrations in (b).

It can be found by trial and error that the functional F describing electroelastic vibrations in a hybrid structure, which consists of two piezoelectric layers, e.g., LiNbO_3 and GaAs layers, takes the form

$$\begin{aligned}
F(U_i^{(1)}; U_i^{(2)}; \Phi^{(1)}; \Phi^{(2)}; V(q)) &= F_1(U_i^{(1)}; \Phi^{(1)}; V(q)) \\
&\quad - \frac{1}{2} \omega^2 \iiint_{\Omega_{R2}} \rho^{(2)} U_i^{(2)} U_i^{(2)} d\Omega \\
&\quad + \frac{1}{2} \iiint_{\Omega_{R2}} g_{i\alpha}^{(2)} g_{j\beta}^{(2)} g_{k\gamma}^{(2)} g_{l\delta}^{(2)} c_{\alpha\beta\gamma\delta}^{E(2)} U_{i,j}^{(2)} U_{k,l}^{(2)} d\Omega \\
&\quad + \iiint_{\Omega_{R2}} g_{m\alpha}^{(2)} g_{k\beta}^{(2)} g_{l\gamma}^{(2)} e_{\alpha\beta\gamma}^{(2)} \Phi_{,m}^{(2)} U_{k,l}^{(2)} d\Omega \\
&\quad - \frac{1}{2} \iiint_{\Omega_{R2}} g_{m\alpha}^{(2)} g_{n\beta}^{(2)} \varepsilon_0 \varepsilon_{\alpha\beta}^{S(2)} \Phi_{,m}^{(2)} \Phi_{,n}^{(2)} d\Omega \\
&\quad + \iint_{S_h} N_j (U_i^{(2)} - U_j^{(1)}) (T_{ij}^{(1)} + T_{ij}^{(2)}) dS \\
&\quad + \iint_{S_h} N_m (\Phi^{(2)} - \Phi^{(1)}) (D_m^{(1)} + D_m^{(2)}) dS, \quad (1)_1
\end{aligned}$$

where the terms describing the LiNbO₃ and GaAs plates are denoted by the upper subscripts 1 and 2, respectively, $U_i^{(1)}$ and $U_i^{(2)}$ are the i -th components of the elastic displacement vectors, $\Phi^{(1)}$ and $\Phi^{(2)}$ are the piezoelectric potentials (assuming their $\exp(j\omega t)$ time dependence), $c_{\alpha\beta\gamma\delta}^{E(1)}$ and $c_{\alpha\beta\gamma\delta}^{E(2)}$ are the components of the elastic tensor taken at a constant electric field strength; $e_{\alpha\beta\gamma}^{(1)}$ and $e_{\alpha\beta\gamma}^{(2)}$ are the components of the piezoelectric tensor, $\varepsilon_{\alpha\beta}^{S(1)}$ and $\varepsilon_{\alpha\beta}^{S(2)}$ are the components of the dielectric tensor taken at a constant value of the elastic strain, ε_0 is the dielectric permittivity of the vacuum, S_h is an electrode – free portion of LiNbO₃ – GaAs interface, N_i and N_j are the components of the normal unit vector directed from layer 1 to layer 2 in Fig. 1a. In writing Eq. (1)₁, the constituent relations for components of the mechanical stress tensors $T_{ij}^{(1,2)}$ and of the electric displacement vectors $D_m^{(1,2)}$ are assumed to be linear in $U_i^{(1,2)}$ and $E_j^{(1,2)} = -\Phi_{,j}^{(1,2)}$, so that

$$\begin{aligned}
T_{ij}^{(1,2)} &= c_{ijkl}^{E(1,2)} U_{k,l}^{(1,2)} + e_{nij}^{(1,2)} \Phi_{,n}^{(1,2)}, \\
D_m^{(1,2)} &= e_{mkl}^{(1,2)} U_{k,l}^{(1,2)} - \varepsilon_0 \varepsilon_{mn}^{S(1,2)} \Phi_{,n}^{(1,2)}.
\end{aligned}$$

The functional F_1 describing vibrations of a LiNbO₃ plate may be expressed as [14]:

$$\begin{aligned}
F_1(U_i^{(1)}; \Phi^{(1)}; V(q)) = & -\frac{1}{2}\omega^2 \iiint_{\Omega_{R1}} \rho^{(1)} U_i^{(1)} U_i^{(1)} d\Omega \\
& + \frac{1}{2} \iiint_{\Omega_{R1}} g_{i\alpha}^{(1)} g_{j\beta}^{(1)} g_{k\gamma}^{(1)} g_{l\delta}^{(1)} c_{\alpha\beta\gamma\delta}^{E(1)} U_{i,j}^{(1)} U_{k,l}^{(1)} d\Omega \\
& + \iiint_{\Omega_{R1}} g_{m\alpha}^{(1)} g_{k\beta}^{(1)} g_{l\gamma}^{(1)} e_{\alpha\beta\gamma}^{(1)} \Phi_{,m}^{(1)} U_{k,l}^{(1)} d\Omega \\
& + \frac{1}{2} \iiint_{\Omega_{R1}} g_{m\alpha}^{(1)} g_{n\beta}^{(1)} \varepsilon_0 \varepsilon_{\alpha\beta}^{S(1)} \Phi_{,m}^{(1)} \Phi_{,n}^{(1)} \\
& - \iiint_{\Omega_{E1}} g_{m\alpha}^{(1)} g_{k\beta}^{(1)} g_{l\gamma}^{(1)} e_{\alpha\beta\gamma}^{(1)} E_{Gm} U_{k,l}^{(1)} d\Omega \\
& - \frac{1}{2} \iiint_{\Omega_{R1}} g_{m\alpha}^{(1)} g_{n\beta}^{(1)} \varepsilon_0 \varepsilon_{\alpha\beta}^{S(1)} E_{Gm} \Phi_{,n}^{(1)} d\Omega \\
& - \frac{1}{2} \iiint_{\Omega_{R1}} g_{m\alpha}^{(1)} g_{n\beta}^{(1)} \varepsilon_0 \varepsilon_{\alpha\beta}^{S(1)} E_{Gm} E_{Gn} d\Omega \\
& + \sum_{p=1}^{Q_E} \iint_{S(p)} N_m(p) g_{m\alpha}^{(1)} g_{k\beta}^{(1)} g_{l\gamma}^{(1)} e_{\alpha\beta\gamma}^{(1)} U_{k,l}^{(1)} [\Phi^{(1)} - V_G(p)] dS \\
& - \sum_{p=1}^{Q_E} \iint_{S(p)} N_m(p) g_{m\alpha}^{(1)} g_{n\beta}^{(1)} \varepsilon_0 \varepsilon_{\alpha\beta}^{S(1)} \Phi_{,n}^{(1)} [\Phi^{(1)} - V_G(p)] dS \\
& + \sum_{q=1}^{Q_F} \iint_{\Sigma(q)} N_m(q) g_{m\alpha}^{(1)} g_{n\beta}^{(1)} g_{l\gamma}^{(1)} e_{\alpha\beta\gamma}^{(1)} U_{k,l}^{(1)} \Phi_{,n}^{(1)} [\Phi^{(1)} - V_G(p)] d\Sigma \\
& - \sum_{q=1}^{Q_F} \iint_{\Sigma(q)} N_m(q) g_{m\alpha}^{(1)} g_{n\beta}^{(1)} \varepsilon_0 \varepsilon_{\alpha\beta}^{S(1)} \Phi_{,n}^{(1)} [\Phi^{(1)} - V_G(p)] d\Sigma, \quad (1)_2
\end{aligned}$$

where $N_m(p)$ and $N_m(q)$ are the m -th components of the unit vectors normal to the p -th exciting and q -th free electrodes, respectively, E_{Gm} is the m -th component of the electric field strength generated within the local volume Ω_{E1} of the

LiNbO₃-plate by the applied signal, implying that the relation $E^{(1,2)}(x, y, z) = -\nabla\Phi^{(1,2)}(x, y, z)$ holds. The subscripts in Eq. (1) vary from 1 to 3 and the Einstein summation convention applies to repeated indices. The coma in the subscript marks differentiation.

Analyzing the free vibrations, one should put $\Omega_{E1} = 0$, $\sum_{p=1}^{Q_E} S(p) = 0$, $V_G(p) = 0$,

and $\mathbf{E}_G = 0$. Furthermore, only the E_G and $V_G(p)$ components written in Eq. (1)₂ are related to forced vibrations. Therefore, when the exciting electrodes shown in Fig. 1a are all arranged on a single face of a plate, the \mathbf{E}_G – components vanish and F_1 reduces to the form given by EERNISSE and HOLLAND [14]. This allows to conclude that the vibration amplitude derived in the case of a surface excitation (when $E_{Gm} = 0$) is much weaker than that one attained with a bulk excitation (when $E_{Gm} \neq 0$).

Equating the first variation of F to zero gives a standard set of equations in terms of eight independent physical functions – $U_X^{(1,2)}(x, y, z)$, $U_Y^{(1,2)}(x, y, z)$, $U_Z^{(1,2)}(x, y, z)$, and $\Phi^{(1,2)}(x, y, z)$. It includes the equation of motion for extensional vibration, and the Maxwell's equation requiring that the divergence of the electric displacement vector is zero. These should be supplemented with the boundary conditions on the plate boundary. On the dielectric part of the boundary, there are no normal components of both the mechanical stress and the electric displacement. On the part of the plate boundary covered with electrodes, the metal layers are considered to be thin and do not influence the above boundary conditions for the stress tensor.

To account for an arbitrary cut resonator plate, the functional F should be generalized by introducing the transition matrix $[g^{(1,2)}]$, which describes the coordinate transformation from the crystallographic system $\{X_C; Y_C; Z_C\}$ to the $\{X; Y; Z\}$ one defined by the plate cut. Then the matrix components $g_{\alpha\beta}$ are [17]

$$[g] = \begin{pmatrix} g_{11} & g_{12} & g_{13} \\ g_{21} & g_{22} & g_{23} \\ g_{31} & g_{32} & g_{33} \end{pmatrix} = \begin{pmatrix} \cos \alpha_2 \cos \alpha_3 & & \\ \sin \alpha_1 \sin \alpha_2 \cos \alpha_3 + \cos \alpha_1 \sin \alpha_3 & & \\ -\cos \alpha_1 \sin \alpha_2 \cos \alpha_3 + \sin \alpha_1 \sin \alpha_3 & & \\ & -\cos \alpha_2 \sin \alpha_3 & \sin \alpha_2 \\ & -\sin \alpha_1 \sin \alpha_2 \sin \alpha_3 + \cos \alpha_1 \cos \alpha_3 & -\sin \alpha_1 \cos \alpha_2 \\ & \cos \alpha_1 \sin \alpha_2 \sin \alpha_3 + \sin \alpha_1 \cos \alpha_3 & \cos \alpha_1 \cos \alpha_2 \end{pmatrix}, \quad (2)$$

where α_1 , α_2 , and α_3 are the rotation angles around the X_C , Y_C and Z_C axes, respectively.

With the electrode configuration shown in Fig. 1b, where the top and the bottom arrangements are mirror-symmetric to each other, the sum of the fifth, sixth and seventh terms in Eq. (1)₂ reduces to

$$\begin{aligned}
& - \iiint_{\Omega_{E1}} g_{m\alpha}^{(1)} g_{k\beta}^{(1)} g_{l\gamma}^{(1)} e_{\alpha\beta\gamma}^{(1)} E_{Gm} U_{k,l}^{(1)} d\Omega + \frac{1}{2} \iiint_{\Omega_{E1}} g_{m\alpha}^{(1)} g_{n\beta}^{(1)} \varepsilon_0 \varepsilon_{\alpha\beta}^{S(1)} E_{Gm} \Phi_{,n}^{(1)} d\Omega \\
& \quad - \frac{1}{2} \iiint_{\Omega_{E1}} g_{m\alpha}^{(1)} g_{n\beta}^{(1)} \varepsilon_0 \varepsilon_{\alpha\beta}^{S(1)} E_{Gm} E_{Gn} d\Omega \\
& = - \sum_{r=1}^{Q_E/2} \left[\frac{V_G(r)}{L_y} \right] \iiint_{\Omega_{E1}(r)} g_{my} g_{k\beta} g_{l\gamma} e_{y\beta\gamma} U_{k,l}^{(1)} d\Omega \\
& + \frac{1}{2} \sum_{r=1}^{Q_E/2} \left[\frac{V_G(r)}{L_y} \right] \iiint_{\Omega_{E1}(r)} (g_{y\alpha} g_{n\beta} \varepsilon_0 \varepsilon_{\alpha\beta}^{S(1)} \Phi_{,n}^{(1)} + g_{m\alpha} g_{y\beta} \varepsilon_0 \varepsilon_{\alpha\beta}^{S(1)} \Phi_{,m}^{(1)}) d\Omega \\
& \quad - \frac{1}{2} \sum_{r=1}^{Q_E/2} \left[\frac{V_G^2(s)}{L_y^2} \right] \iiint_{\Omega_{E1}(r)} g_{y\alpha} g_{y\beta} \varepsilon_0 \varepsilon_{\alpha\beta}^{S(1)} d\Omega.
\end{aligned}$$

Basing on the above formulation, the free vibrations of a 128°-Y-rotated LiNbO₃ rectangular plate with the rotation angles $\alpha_1 = 128^\circ$, $\alpha_2 = 0^\circ$ and $\alpha_3 = 0^\circ$ are then analyzed in three cases which are as follows (see Fig. 2).

1. The plate surfaces are uncovered with metal electrodes, so $x_1 = x_2 = L_X/2$ and $z_1 = z_2 = L_Z/2$.
2. A pair of open-circuited electrodes fully covers the opposite XZ -planes of the plate, so $x_1 = x_2 = 0$ and $z_1 = z_2 = 0$.
3. A pair of open-circuited electrodes partly covers the opposite XZ -planes of the plate such that $x_1 = x_2 < L_X/2$ and $z_1 = z_2 = 0$.

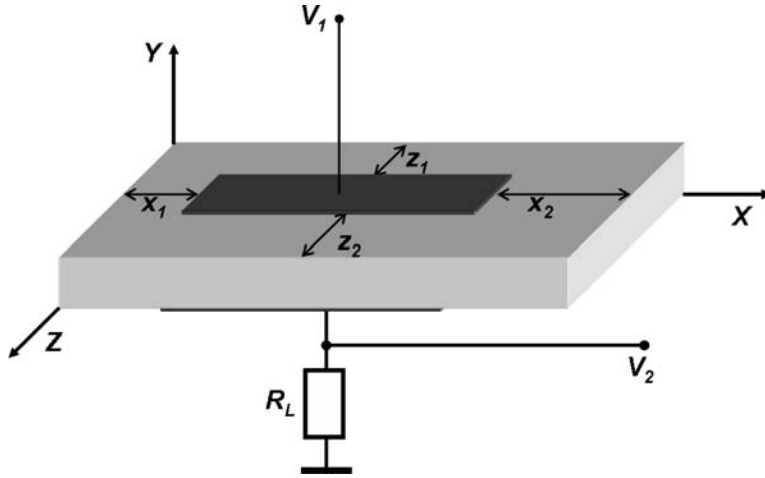


Fig. 2. Scheme of the impedance setup showing a LiNbO₃ plate (shaded body) oriented along the X-, Y- and Z-axes, metal electrodes (filled rectangles), the load resistance R_L , the input voltage V_1 and output one V_2 .

Within the Rayleigh–Ritz calculation procedure, in order to minimize the F one should expand the $U_X^{(1,2)}(x, y, z)$, $U_Y^{(1,2)}(x, y, z)$, $U_Z^{(1,2)}(x, y, z)$, and $\Phi^{(1,2)}(x, y, z)$ functions in series over a set of trial functions which must be complete and linear independent, and also continuous and doubly differentiable [24]. The series expansions have been constructed in the following form:

$$\begin{aligned}
 U_X^{(1,2)}(x, y, z) &= \sum_{\alpha=1}^{Q_U} B^{(1,2)}(\alpha) BF_1(\alpha, x, y, z) \\
 &= \left(\sum_{\alpha=1}^{Q_{U1}} B^{(1,2)}(\alpha) TF_{11}(\alpha, x, y, z) + \sum_{\alpha=1}^{Q_{U2}} B^{(1,2)}(\alpha) TF_{12}(\alpha, x, y, z) \right) \\
 &\quad \cdot WF(K_X, K_Z, x, z), \\
 U_Y^{(1,2)}(x, y, z) &= \sum_{\alpha=Q_U+1}^{2Q_U} B^{(1,2)}(\alpha) BF_2(\alpha, x, y, z) \\
 &= \left(\sum_{\alpha=Q_U+1}^{Q_{U2}} B^{(1,2)}(\alpha) TF_{21}(\alpha, x, y, z) + \sum_{\alpha=Q_{U2}+1}^{2Q_U} B^{(1,2)}(\alpha) TF_{22}(\alpha, x, y, z) \right) \\
 &\quad \cdot WF(K_X, K_Z, x, z), \\
 U_Z^{(1,2)}(x, y, z) &= \sum_{\alpha=2Q_U+1}^{3Q_U} B^{(1,2)}(\alpha) BF_3(\alpha, x, y, z) \\
 &= \left(\sum_{\alpha=2Q_U+1}^{Q_{U3}} B^{(1,2)}(\alpha) TF_{31}(\alpha, x, y, z) + \sum_{\alpha=Q_{U3}+1}^{3Q_U} B^{(1,2)}(\alpha) TF_{32}(\alpha, x, y, z) \right) \\
 &\quad \cdot WF(K_X, K_Z, x, z), \\
 \Phi^{(1,2)}(x, y, z) &= \sum_{\beta=1}^{Q_\Phi} C^{(1,2)}(\beta) BF_4(\beta, x, y, z) \\
 &= \left(\sum_{\beta=1}^{Q_{\Phi1}} C^{(1,2)}(\beta) TF_{41}(\beta, x, y, z) + \sum_{\beta=Q_{\Phi1}+1}^{Q_{\Phi2}} C^{(1,2)}(\beta) TF_{42}(\beta, x, y, z) \right. \\
 &\quad \left. + \sum_{\beta=Q_{\Phi2}+1}^{Q_\Phi} C^{(1,2)}(\beta) TF_{43}(\beta, x, y, z) \right) WF(K_X, K_Z, x, z).
 \end{aligned} \tag{3}$$

In Eqs. (3)₁₋₃, the trigonometric trial functions $TF_{ij}(x, y, z)$ ($i = 1, 2, 3$) are taken from Table 2 in [12]. It is convenient to approximate the potential $\Phi^{(1,2)}$ with

$$\begin{aligned} TF_{41}(\beta, x, y, z) &= \sin\left(\frac{\pi M_{4S}(\beta)}{L_X^{(1)}}x\right) \cos\left(\frac{\pi N_{4C}(\beta)}{L_Y^{(1)} + L_Y^{(2)}}y\right) \cos\left(\frac{\pi P_{4C}(\beta)}{L_Z^{(1)}}z\right), \\ TF_{42}(\beta, x, y, z) &= \cos\left(\frac{\pi M_{4C}(\beta)}{L_X^{(1)}}x\right) \sin\left(\frac{\pi N_{4S}(\beta)}{L_Y^{(1)} + L_Y^{(2)}}y\right) \cos\left(\frac{\pi P_{4C}(\beta)}{L_Z^{(1)}}z\right), \\ TF_{43}(\beta, x, y, z) &= \sin\left(\frac{\pi M_{4S}(\beta)}{L_X^{(1)}}x\right) \sin\left(\frac{\pi N_{4S}(\beta)}{L_Y^{(1)} + L_Y^{(2)}}y\right) \sin\left(\frac{\pi P_{4S}(\beta)}{L_Z^{(1)}}z\right). \end{aligned} \quad (4)$$

Here, the integers $M_{kS}(\alpha)$, $M_{kC}(\alpha)$, $N_{kS}(\alpha)$, $N_{kC}(\alpha)$, $P_{kS}(\alpha)$ and $P_{kC}(\alpha)$ are the coordinate characteristic numbers (CCNs), and the number of the trial functions is defined by Q_U and Q_Φ . Following the landmark paper [12], the integers in the $\{M_{kS}(\alpha), M_{kC}(\alpha)\}$ -, $\{N_{kS}(\alpha), N_{kC}(\alpha)\}$ -, and $\{P_{kS}(\alpha)$ and $P_{kC}(\alpha)\}$ -pairs are chosen so as to be of the opposite parities, namely, {odd, even} or {even, odd}. The $B(\alpha)$ and $C(\beta)$ coefficients are estimated by a standard procedure [14].

Apparently, there are two important issues in constructing the trial functions needed for characterizing the vibrations of the resonators which are partly covered by electrodes. First, a new view emerges from the terms $TF_{41}(x, y, z)$ and $TF_{42}(x, y, z)$ which are introduced in Eq. (4) in order to account for the penetration of the electric field outside the vibrating plate. Previously, the expansion of the Φ function into series of two TF_{4j} components including the $\sin(\dots) \cdot \sin(\dots) \cdot \sin(\dots)$ and $\cos(\dots) \cdot \cos(\dots) \cdot \sin(\dots)$ terms [12] was only capable to describe the vibrations of a short-circuited piezoelectric plate covered fully with electrodes.

Second, a proper understanding requires taking into account the wave-factor $WF(K_X, K_Y, x, z)$ included in Eq. (3) (only for the $U_X^{(1)}(x, y, z)$, $U_Y^{(1)}(x, y, z)$, $U_Z^{(1)}(x, y, z)$, and $\Phi^{(1)}(x, y, z)$ functions). This comes from the plate waves traversing the plate which are likely to appear if the electrode area is remarkably small thus making a significant contribution to the vibration properties of the plate [5]. Setting $WF(K_X, K_Z, x, z) = 1$ allows to attain a large-electrode area case.

For definiteness, suppose the waves are purely standing ones and assume their reflections at the edges of the plate are loss-free. Then

$$\begin{aligned} WF(K_X, K_Z, x, z) &= WF_1(K_X, x) \cdot WF_2(K_Z, z), \\ WF_1(K_X, x) &= \frac{1}{2} \{ \cos(K_X \cdot x) + \cos[K_X(L_X - x)] \}, \\ WF_2(K_Z, z) &= \frac{1}{2} \{ \cos(K_Z \cdot z) + \cos[K_Z(L_Z - z)] \}, \end{aligned} \quad (5)$$

where $K_X = \omega/V_X(\omega)$ and $K_Z = \omega/V_Z(\omega)$ are the X - and Z -components of the wave vector, respectively, and V_X and V_Z are the corresponding components of the wave phase velocity.

Turning to the trial functions introduced here it should be noted that the sets of $\{TF_{11}, TF_{12}\}$, $\{TF_{21}, TF_{22}\}$, $\{TF_{31}, TF_{32}\}$, and $\{TF_{41}, TF_{42}, TF_{43}\}$ are neither orthogonal nor complete, although, taken separately, each of the sets $\{TF_{ij}\}$ definitely satisfies the general demand of the orthogonality and completeness. As remarked previously, such ‘‘overcomplete’’ sets of the trial functions accelerate the convergence of the series (3) in the computations [13]. Meanwhile, the mathematics behind this problem is well beyond the scope of the present work. Concerning the wave-factor WF given above, it is easy to show that, for $K_X L_X = \pi N_X$ or $K_Z L_Z = \pi N_Z$ ($N_X, N_Z = 1, 2, \dots$), which are only of practical relevance since in these cases the surface distributions of the elastic and electric fields are remarkably affected by the $WF(K_X, K_Z, x, z)$ wave factor, the $\{BF_{ij}\}$ trial function sets remain complete and orthogonal. Therefore, the computation results require further experimental evidence to secure the validity of the trial functions introduced above. As shown below, the principal findings of experimental vibration frequencies match the expectations of this theory thus supporting the theoretical approach.

When treating the vibration problem variationally for a particular vibration mode, the distributions of U_X , U_Y , U_Z and Φ over the surface of a vibrating structure are defined by a proper choice of the odd (‘‘O’’) and even (‘‘E’’) parities, which are assigned to the corresponding CCN [12]. Taking U_Z component as an example, this can be written as

$$\begin{aligned} U_Z(L_X, y, z) &= U_Z(0, y, z) && \text{for even} && M_Z(\alpha), \\ U_Z(L_X, y, z) &= -U_Z(0, y, z) && \text{for odd} && M_Z(\alpha), \end{aligned}$$

due to the presence of the cos-components in the expansion of U_Z given in Table 2 of [12]. These formulas indicate that asymmetric and symmetric $U_Z(X)$ distributions occur. Speaking more generally, there would be eight parity sets $\{R1; R2; R3; R4; R5; R6; R7; R8\}$ for the CCN triplet of $\{M_k(\alpha), N_k(\alpha), P_k(\alpha)\}$ in the trial function $TF_{ij}(x, y, z)$. Then $R1 = (E, E, E)$, $R2 = (O, E, E)$, $R3 = (E, O, E)$, $R4 = (E, E, O)$, $R5 = (E, O, O)$, $R6 = (O, E, O)$, $R7 = (O, O, E)$ and $R8 = (O, O, O)$, where the first parity is ascribed to the X -coordinate CCN, the second one – to that of the Y -coordinate, and the third one – to that of the Z -coordinate. Therefore, to model the plate vibrations, taking into account the opposite parities of the CCN pairs, four parity sets Rn corresponding to twelve CCNs in Eqs. (3) should be specified for every vibration mode. In general, the total number of the twelve parity combinations is $2^{12} = 4096$. Taking into account the deformation symmetry of the crystal it is possible to get the permitted combinations of symmetrical and antisymmetrical distributions of U_X , U_Y , U_Z and Φ which substantially decreases the number of parity choices for CCNs in

Eqs. (3). This in turn determines the vibration modes that are only sustained in the parallelepiped of a given crystallographic class.

For example, eight allowed vibration modes of a piezoceramic parallelepiped were described by HOLLAND [12] in terms of trigonometric trial functions. Four vibration modes were obtained in a cubic-shaped Z -rotated cut LiNbO₃, although the lowest overtones of only one of the modes were observed experimentally at a point mechanical excitation [22]. Thus, it may be concluded that the excitation of vibrations in a given mode for an arbitrarily cut LiNbO₃ resonator remains a challenging task, both theoretically and experimentally.

In what follows, two questions are addressed:

1. Which vibration modes can be excited with a given electrode configuration?
2. Which electrode configuration and distribution of the input signals over the electrodes allow to support a given vibration mode?

The fifth and sixth terms in the functional F_1 are the key to answering these questions. In general, the electrical excitation of the vibrations is possible if the two terms are nonzero ones. It might be expected that the number of modes supported by the plate takes its minimum value using the \mathbf{E}_G exciting field with only one nonzero component. This case can be realized, for example, in the geometry shown in Fig. 1b if the inter-electrode spacing is large enough to give

$$\iiint_{\Omega_{E1}} g_{m\alpha}^{(1)} g_{k\beta}^{(1)} g_{l\gamma}^{(1)} e_{\alpha\beta\gamma}^{(1)} U_{k,l}^{(1)} d\Omega \neq 0 \quad (6)$$

for TF_{1i} , TF_{2i} and TF_{3i} (Table 2 in [12]) with $\alpha = 1, 2$, and 3 for the YZ -, XZ - and XY -faces, respectively; and

$$\iiint_{\Omega_{E1}} (g_{k\alpha}^{(1)} g_{n\beta}^{(1)} \varepsilon_0 \varepsilon_{\alpha\beta}^{S(1)} \Phi_{,n}^{(1)} + g_{m\alpha}^{(1)} g_{n\beta}^{(1)} \varepsilon_0 \varepsilon_{\alpha\beta}^{S(1)} \Phi_{,m}^{(1)}) d\Omega \neq 0 \quad (7)$$

for TF_{4j} (see Eq. (4)) with $k = 1, 2$ and 3 for the YZ -, XZ -, and XY -faces, respectively. Noticeably, relations (6) and (7) are applicable to a piezocrystal plate of any crystallographic class, standing as a criterion mediating between the electrically-excited and non-excited vibration modes.

Substituting the trial functions modelling $U_i^{(1)}$ and $\Phi^{(1)}$ into (6) and (7) and integrating over Ω_{E1} , which is defined by the electrode configuration, one takes the parity sets related to the excited vibration modes. Alternatively, the parity sets forcing the integrals in formulas (6) and (7) to be zero define non-piezoelectric vibration modes which therefore can not be electrically excited. This analysis allows to choose correctly the parity sets pertinent to the measured frequency spectrum, but requires further experimental evidence to answer the question if the mode is non-degenerate or not.

Some of the computation results are summarized in Table 1. Here are given the parity sets Rn for the vibration modes of a 128°- Y -rotated cut LiNbO₃ rectangular plate which is electrically excited with a single pair of rectangular-shaped

Table 1. The parity sets Rn for the trial functions $TF0_{ij}$ used to model the extensional vibration modes electrically excited in a 128° - Y -rotated LiNbO_3 rectangular-plate resonator with a pair of rectangular-shaped electrodes located asymmetrically (A) or symmetrically (B) on its opposite faces. Electrode's dimensions are given in the first column.

	For $TF0_{1i}$	For $TF0_{2i}$	For $TF0_{3i}$	For $TF0_{4j}$	
(A) Asymmetric location					
(A1) Electrodes are on XY -faces					
$x_1 = x_2 = 0, y_1 = y_2 = 0$	$R5$	$R6$	$R7$	$R5, R7$	2
$x_1 \neq x_2, y_1 = y_2 = 0$	$R5, R8$	$R4, R6$	$R3, R7$	$R3, R5, R7, R8$	32
$x_1 = x_2 = 0, y_1 \neq y_2$	$R4, R5$	$R6, R8$	$R2, R7$	$R2, R4, R5, R7$	32
$x_1 \neq x_2, y_1 \neq y_2$	$R4, R5, R6, R8$	$R4, R5, R6, R8$	$R2, R3, R7, R8$	$R1, R2, R3, R4, R5, R6, R7, R8$	512
(A2) Electrodes are on XZ -faces					
$x_1 = x_2 = 0, z_1 = z_2 = 0$	$R5$	$R6$	$R7$	$R6$	1
$x_1 \neq x_2, z_1 = z_2 = 0$	$R5, R8$	$R4, R6$	$R3, R7$	$R4, R6$	16
$x_1 = x_2 = 0, z_1 \neq z_2$	$R3, R5$	$R2, R6$	$R7, R8$	$R2, R6$	16
$x_1 = x_2 = 0, z_1 = z_2 = 0$	$R5$	$R6$	$R7$	$R6$	1
(A3) Electrodes are on YZ -faces					
$y_1 = y_2 = 0, z_1 = z_2 = 0$	$R5$	$R6$	$R7$	$R5, R7$	2
$y_1 \neq y_2, z_1 = z_2 = 0$	$R4, R5$	$R6, R8$	$R2, R7$	$R2, R4, R5, R7$	32
$y_1 = y_2 = 0, z_1 \neq z_2$	$R3, R5$	$R2, R6$	$R7, R8$	$R3, R5, R7, R8$	32
$y_1 \neq y_2, z_1 \neq z_2$	$R1, R2, R4, R5$	$R2, R6, R7, R8$	$R2, R6, R7, R8$	$R1, R2, R3, R4, R5, R6, R7, R8$	512
(B) Symmetric location					
(B1) Electrodes are on XY -faces					
$x_1 = x_2 \neq 0, y_1 = y_2 = 0$	$R5$	$R6$	$R7$	$R5, R7$	2
$x_1 = x_2 = 0, y_1 = y_2 \neq 0$	$R5$	$R6$	$R7$	$R5, R7$	2
$x_1 = x_2 \neq 0, y_1 = y_2 \neq 0$	$R5$	$R6$	$R7$	$R5, R7$	2
(B2) Electrodes are on XZ -faces					
$x_1 = x_2 \neq 0, z_1 = z_2 = 0$	$R5$	$R6$	$R7$	$R6$	1
$x_1 = x_2 = 0, z_1 = z_2 \neq 0$	$R5$	$R6$	$R7$	$R6$	1
$x_1 = x_2 \neq 0, z_1 = z_2 \neq 0$	$R5$	$R6$	$R7$	$R6$	1
(B3) Electrodes are on YZ -faces					
$y_1 = y_2 \neq 0, z_1 = z_2 = 0$	$R5$	$R6$	$R7$	$R5, R7$	2
$y_1 = y_2 = 0, z_1 = z_2 \neq 0$	$R5$	$R6$	$R7$	$R5, R7$	2
$y_1 = y_2 \neq 0, z_1 = z_2 \neq 0$	$R5$	$R6$	$R7$	$R5, R7$	2

electrodes (see Fig. 2). To determine the parity sets substitute $\alpha = 2$ and $k = 2$ in formulas (6) and (7), respectively, so the integration reduces to

$$\iiint_{\Omega_{E1}} (...) d\Omega \rightarrow \int_{x1}^{L_X^{(1)}-x2} dx \int_0^{L_Y^{(1)}} dy \int_{z1}^{L_Z^{(1)}-z2} (...) dz.$$

All the Rn sets given in Table 1 correspond to the trial function of the form

$$TF0_{ki}(x, y, z) = \sin[\pi m_{ki}(\alpha)x/L_X^{(1)}] \cdot \sin[\pi n_{ki}(\alpha)y/L_Y^{(1)}] \cdot \sin[\pi p_{ki}(\alpha)/L_Z^{(1)}]$$

with $i = 1$ and 2 for $k = 1, 2$ and 3 , and $i = 1, 2$ and 3 for $k = 4$, since the $\{M_{kS}(\alpha), M_{kC}(\alpha)\}$ -, $\{N_{kS}(\alpha), N_{kC}(\alpha)\}$ -, and $\{P_{kS}(\alpha)$ and $P_{kC}(\alpha)\}$ - pairs are of opposite parities. In terms of the parity sets $\{R1; R2; R3; R4; R5; R6; R7; R8\}$, each extensional vibration mode can be described by

$$\begin{aligned} \{Ri \text{ (for } TF0_1), Rj \text{ (for } TF0_2), Rk \text{ (for } TF0_3), Rl \text{ (for } TF0_4)\} \\ \equiv \{Ri, Rj, Rk, Rl\}(i, j, k, l = 1, 8). \end{aligned}$$

Then the case of $x_1 = x_2$ and $z_1 = z_2$ in Fig. 2 is referred to as the symmetric electrode configuration. Otherwise, it is non-symmetric. In case of the multiple pairs of electrodes shown in Fig. 1a, the electrode configuration is symmetric if the bottom- and top-faced electrodes are mirrored with respect to the middle plane of the plate.

Obviously, the non-symmetric electrode configurations produce a greater number of vibration modes due to a greater number of the nonzero E_G components; see Eq. (1). The number of various vibration modes supported by a given electrode configuration is summarized in the last column of Table 1. However, there is one significant issue that will need further work: it is still unclear which of the modes are non-degenerated giving rise to different eigenfrequency spectra. Apparently, a better understanding requires taking into account several different vibration modes that can be excited simultaneously at a given frequency. In this case, the elastic displacements and the piezoelectric potential can be expanded over the normal vibration modes as illustrated, e.g. in [14, 23].

In order to check the consistency of the results, the eigenfrequencies of the lithium niobate vibrating plates taken experimentally are then compared with those obtained theoretically.

3. Samples

Experiments were performed on two samples, LNO-1 and LNO-4a, of a 128°-Y-rotated cut lithium niobate ($\{\alpha_1, \alpha_2, \alpha_3\} = \{128^\circ, 0^\circ, 0^\circ\}$) which is typically used for guiding the surface acoustic waves [26]. They have been investigated experimentally. The samples were rectangular shaped with linear dimensions L_X ,

L_Y and L_Z given in Table 2. A measure of the nonuniformity in L_i defined as $\Delta L_i = L_{i,\max} - L_{i,\min}$ with $i = x, y, z$ is tabulated as well.

Table 2. Sample's average linear dimensions (\bar{L}_i) and related nonuniformities (ΔL_i) (in mm).

Sample	\bar{L}_x	ΔL_x	\bar{L}_y	ΔL_y	\bar{L}_z	ΔL_z
LNO-1	13.45	0.01	0.775	0.005	3.64	0.01
LNO-4a	19.20	0.015	0.70	0.01	3.61	0.01

Electroelastic vibrations were excited with a pair of thin metallic electrodes formed by a fine-dispersive Ag powder deposited on the opposite XZ -planes of the samples. The tangent of the dielectric loss, measured at the frequency of 1 kHz, did not exceed 5×10^{-3} . Care was taken to ensure the stability of the electrical input and output contacts attached to the electrodes and to achieve the traction-free mechanical condition at the surfaces of the plate.

4. Eigenfrequency measurements

The eigenfrequencies of the samples were taken by using the standard impedance technique [3] schematically sketched in Fig. 2. Taking the R_L to be much greater than the real part $\text{Re}\{\dot{Z}(f)\}$ of the sample's electric impedance $\dot{Z}(f)$, this results in

$$\left| \dot{Y}(f) \right| \approx R_L \cdot \left| \dot{V}_2(f) / \dot{V}_1(f) \right|,$$

where $\dot{Y}(f) = \dot{Z}^{-1}(f)$ is the complex conductivity of the piezoelectric resonator and the voltages V_1 and V_2 are shown in Fig. 2. Then the frequency dependence of $|\dot{Y}(f)|$ represents the sample's eigenfrequency spectrum [4]. This was found to change with varying the values of x_1 , x_2 , z_1 and z_2 shown in Fig. 2.

5. Experimental results and discussion

The frequency dependence $|\dot{Y}(f)|$ taken in the sample LNO-1 fully covered with electrodes (i.e. $x_1 = x_2 = 0$ and $z_1 = z_2 = 0$ in Fig. 2) is shown in Fig. 3. A number of maxima and minima reflecting an overtone's family of a vibration mode (or, maybe, of several modes) is clearly resolved. The measured frequencies $f_{rE}(n)$, corresponding to maxima in Fig. 3, are the parallel-resonance frequencies of the sample with n being the serial number of an overtone. The minima $f_{aE}(n)$ give the sample's series-resonance (or antiresonant) frequencies. It is known [1] that the eigenfrequency spectrum of a piezoelectric resonant structure is represented by either the $f_r(n)$ set for the short-circuited electrodes or the $f_a(n)$ set for the open-circuited ones. Theoretically, the setup displayed in Fig. 2 is considered

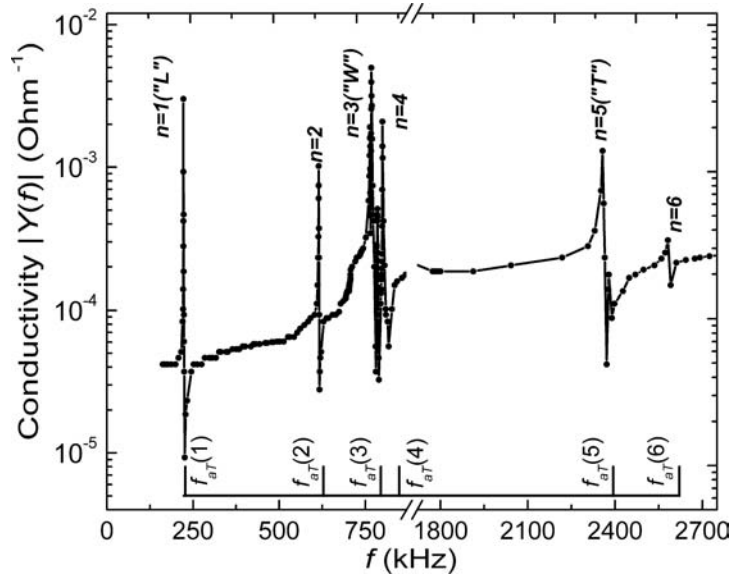


Fig. 3. Frequency dependence of the complex conductivity $|Y(f)|$ taken in the sample LNO-1 (solid curve). The computed antiresonant frequencies $f_{aT}(n)$ are marked below the curve.

to be open-circuited. The most significant resonant and antiresonant frequencies taken in our samples are summarized in Table 3.

This way of looking at the experimental results can be given supporting ev-

Table 3. A comparison between the experimentally measured frequencies $f_{aE}(n)$ and the computed ones $f_{aT}(n)$ for LNO-1 and LNO-4a samples. The frequencies $f_{aT}(n)$ are calculated with $Q_U = Q_\Phi = 33$ for the $\{R5, R6, R7, R6\}$ -vibration mode.

Overtone's serial number n						
	$n = 1$ ("L")	$n = 2$	$n = 3$ ("W")	$n = 4$	$n = 5$ ("T")	$n = 6$
Sample LNO-1						
$f_{rE}(n)$, kHz	222.2	614.8	768.0	799.9	2357.1	2581.6
$f_{aE}(n)$, kHz	226.1	617.3	781.1	830.8	2371.2	2591.0
$f_{aT}(n)$, kHz	227.3	643.0	793.4	826.2	2408.0	2570.5
$\Delta_1(n)$, %	0.5	3.9	1.5	0.6	1.6	0.8
Sample LNO-4a						
$f_{rE}(n)$, kHz	158.3	461.5	731.6	764.1	2259.8	2492.8
$f_{aE}(n)$, kHz	160.3	462.0	738.9	782.4	2291.1	2503.7
$f_{aT}(n)$, kHz	159.5	472.4	723.3	795.9	2327.6	2562.6
$\Delta_1(n)$, %	0.5	2.2	2.1	1.7	1.6	2.3

Table 4. The experimentally measured frequencies $f_{aE}(n)$, and the computed ones $f_{aT}(n)$, for various values of the electrode's area (sample LNO-1, symmetric configuration of electrodes).

Overtone's serial number n						
	$n = 1$ ("L")	$n = 2$	$n = 3$ ("W")	$n = 4$	$n = 5$ ("T")	$n = 6$
Calculated values $f_{aT}(n)$ [kHz] ($Q_U = Q_\Phi = 33$, the $\{R5, R6, R7, R6\}$ – vibration mode)						
Non-metallized faces	229.6	683.1	822.9	877.1	2583.0	2667.5
70%-metallized	227.8	652.7	804.9	843.0	2526.1	2625.3
100%-metallized	227.3	643.0	793.4	826.2	2408.7	2570.5
$\delta f_{aT}(n)$, kHz	0.2	1.5	1.45	2.0	4.8	2.1
Measured values $f_{aE}(n)$, kHz						
70%-metallized	227.1	620.6	788.9	838.5	2392.6	2607.0
100%-metallized	226.1	617.3	781.1	830.8	2371.2	2591.0
$\delta f_{aE}(n)$, kHz	0.4	0.5	1.0	0.9	0.9	0.6

idence by using the computation work performed here. The computed $f_{aT}(n)$ and the measured $f_{rE}(n)$ and $f_{aE}(n)$ frequencies are contrasted in Table 3. In the plate with fully metallized XZ -planes, the $\{R5, R6, R7, R6\}$ - vibration mode should be analyzed; see second row [part (B2)] in Table 1. Computing the eigenfrequencies, the material constants $c_{ij}^{E(1)}$, $e_{mn}^{(1)}$, and $\varepsilon_{kl}^{S(1)}$ are taken from SMITH and WELSH [30]. The spectrum $f_{aT}(n)$ is obtained with $Q_U = Q_\Phi = 33$. Following the classification scheme given above the $R8$ and $R2$ parity sets are used for the TF_{11} and TF_{12} trial functions, $R8$ and $R3$ – for TF_{21} and TF_{22} , $R8$ and $R4$ – for TF_{31} and TF_{32} , $R7$, $R1$ and $R6$ – for TF_{41} , TF_{42} and TF_{43} , respectively.

Comparing the measured and computed eigenfrequencies given in Table 3, a few percent discrepancy is seen which can be due to two main factors. The first one comes from the non-uniformity of the sample dimensions (see ΔL_X , ΔL_Y and ΔL_Z in Table 2). Evidently, the decrease in L_i across the plate increases $f_{aT}(n)$. For example, a 1% decrease (increase) in L_X , L_Y and L_Z yields the frequency $f_{aT}(1)$ increase (decrease) of about 1% in the sample LNO-1. Also, the non-uniformity produces a departure $\Delta\alpha_i$ from the angles α_i defining the crystallographic cut of the sample. Taking $\Delta\alpha_1 \approx 1^\circ$, $\Delta\alpha_2 \approx 1^\circ$, $\Delta\alpha_3 \approx 1^\circ$ in the sample LNO-1 results in a $f_{aT}(1)$ frequency shift from 227.3 to 227.2 kHz for $\{\alpha_1, \alpha_2, \alpha_3\} = \{129^\circ, 1^\circ, 1^\circ\}$. If $\{\alpha_1, \alpha_2, \alpha_3\} = \{127^\circ, -1^\circ, -1^\circ\}$ the frequency shifts from 227.3 to 227.4 kHz. Secondly, the values of the material constants are not definitely known. Then, varying $c_{ij}^{E(1)}$, $e_{mn}^{(1)}$, and $\varepsilon_{kl}^{S(1)}$ within $\pm 1\%$ leads to the $f_{aT}(1)$ shift of about $\pm 0.5\%$ in the sample LNO-1. Therefore, a comparison of the observed frequency spectrum with variational calculations, using the functional and the trial functions given above, allows to identify the majority of the peaks shown in Fig. 3. However, there exist fine structures in the frequency spectra

that still can not be explained. For example, the peak marked by “W” in Fig. 3 exhibits a triplet structure: it is accompanied by two subsidiary peaks on its low- and high-frequency sides. The explanation may lie in additional effects, such as the coupling between the tone and flexural vibration modes, which are beyond the scope of the present work.

Experiments show a significant systematic effect of decreasing eigenfrequencies with increasing metallization surface area, which is supported by the computations. One example is shown in Table IV where the frequency spectra obtained both theoretically and experimentally are given for two symmetric electrode configurations (see Fig. 2). They are fully-metallized XZ -faces with $x_1 = x_2 = 0$ mm and $z_1 = z_2 = 0$ mm, and $\approx 70\%$ -metallized XZ -faces with $x_1 = x_2 = 2$ mm and $z_1 = z_2 = 0$ mm. Here, the results are contrasted with that obtained for the non-metallized sample. It is seen that, at any given overtone serial number n , metallization decreases both the f_{aT} and f_{aE} frequencies.

6. Conclusions

The following conclusions can be drawn from the presented analysis:

1. The problem of the free and forced (electrically excited) extensional vibrations in a three-dimensional hybrid structure composed of two rectangular piezoelectric plates of arbitrary cuts can be solved variationally by using the generalized functional, quadratic in the elastic displacement components and the piezoelectric potential, proposed in this work.
2. A good agreement between the measured and computed antiresonant frequencies in a 128°- Y -rotated cut LiNbO₃ rectangular plate covered with electrodes is obtained for a few lowest overtones in the electrically excited vibration mode.
3. The natural frequencies of the extensional vibration mode overtones are found, both experimentally and theoretically, to decrease with increasing area of the exciting electrodes.

Acknowledgment

We are grateful to Eugen V. Psyarnetsky and Eugen O. Melezhyk for their assistance in making measurements.

References

- [1] ALLIK H., HUGHES T.J.R., *Finite element method for piezoelectric vibration*, Int. J. Num. Meth. Eng., **2**, 150–157 (1970).
- [2] ALLIK H., WEBMAN K.M., HUNT J.T., *Vibrational response of sonar transducers using piezoelectric finite elements*, J. Acoust. Soc. Amer., **56**, 1782–1791 (1974).

- [3] BERLINCOURT D.A., CURRAN D.R., JAFFE H., *Piezoelectric and Piezomagnetic Materials and Their Function in Transducers*, [In:] Physical Acoustic MASON W.P. [Ed.], vol. 1, part. A, pp. 169–270, Academic Press, New York 1964.
- [4] DU XIAO-HONG, WANG QING-MING, UCHINO K., *Accurate determination of complex materials coefficients of piezoelectric resonators*, IEEE Trans. on Ultrasonics, Ferroelectrics and Frequency Control, **50**, 312–320 (2003).
- [5] FRIEDRICH W., LERCH R., PRESTELE, SOLDNER R., *Simulations of piezoelectric Lamb wave delay lines using a finite element K. method*, IEEE Trans. on Ultrasonics, Ferroelectrics and Frequency Control, **37**, 248–254 (1990).
- [6] GORB A.M., NADTOCHII A.B., KOROTCHENKOV O.A., *Motion of microscopic grains in a periodic potential of plate acoustic waves*, J. Phys.: Condens. Matt., **15**, 7201–7211 (2003).
- [7] GOVOROV A.O., KALAMEITSEV A.V., ROTTER M., WIXFORTH A., KOTTHAUS J.P., HOFFMANN K.-H., BOTKIN N., *Nonlinear Acoustoelectric Transport in a Two-Dimensional Electron System*, Phys. Rev. B 62 2659–2668, and references therein (2000).
- [8] GUO N., CAWLEY P., *Measurement and prediction of the frequency spectrum of piezoelectric disks by modal analysis*, J. Acoust. Soc. Amer., **92**, 3379–3388 (1992).
- [9] HAYLIGER P., *Traction-free vibration of layered elastic and piezoelectric rectangular parallelepipeds*, J. Acoust. Soc. Amer., **107**, 1235–1245 (2000).
- [10] HEYLIGER P., SARAVANOS D.A., *Exact free-vibration analysis of laminated plates with embedded piezoelectric layers*, J. Acoust. Soc. Amer., **98**, 1547–1557 (1995).
- [11] HAYWARD G., GILLIES D., *Block diagram modeling of tall, thin parallelepiped piezoelectric structures*, J. Acoust. Soc. Amer., **86**, 1643–1653 (1989).
- [12] HOLLAND R., *Resonant properties of piezoelectric ceramic rectangular parallelepipeds*, J. Acoust. Soc. Am., **43**, 988–997 (1968a).
- [13] HOLLAND R., *Contour extensional resonant properties of rectangular piezoelectric plates*, IEEE Trans. Sonics and Ultrasonics, **15**, 97–105 (1968b).
- [14] HOLLAND R., EER NISSE, *Variational evaluation of admittances of multielectroded three-dimensional piezoelectric structures*, IEEE Trans. Sonics and Ultrasonics, SU-15, 119–132 (1968).
- [15] HUANG C.-H., MA C.-C., *Experimental and numerical investigations of resonant vibration characteristics for piezoceramic plates*, J. Acoust. Soc. Amer., **109**, 2780–2788 (2001).
- [16] IKEGAMI S., UEDA I., KOBAYASHI S., *Frequency spectra of resonant vibration in disk plates of PbTiO₃ piezoelectric ceramics*, J. Acoust. Soc. Amer., **55**, 339–344 (1974).
- [17] KORN A., KORN T.M., *Mathematical Handbook for Scientists and Engineers*, McGraw-Hill, New York 1968.
- [18] KUNKEL H.A., LOCKE S., PIKEROEN B., *Finite-element analysis of vibrational modes in piezoelectric ceramic disks*, IEEE Trans. on Ultrasonics, Ferroelectrics and Frequency Control, **37**, 316–328 (1990).
- [19] LERCH R., *Simulation of piezoelectric devices by two- and three-dimensional finite elements*, IEEE Trans. on Ultrasonics, Ferroelectrics and Frequency Control, **37**, 233–247 (1990).

-
- [20] LIN Y.-C., MA C.-C., *Experimental measurement and numerical analysis on resonant characteristics of piezoelectric disks with partial electrode designs*, IEEE Trans. on Ultrasonics, Ferroelectrics and Frequency Control, **51**, 937–947 (2004).
- [21] MA C.-C., HUANG C.-H., *The investigation of three-dimensional vibration for piezoelectric rectangular parallelepipeds using the AF-ESPI method*, IEEE Trans. on Ultrasonics, Ferroelectrics and Frequency Control, **48**, 142–153 (2001).
- [22] OGI H., KAWASAKI Y., HIRAO M., *Acoustic spectroscopy of lithium niobate: Elastic and piezoelectric coefficients*, J. Appl. Phys., **92**, 2451–2456 (2002).
- [23] PEACH R.C., *A normal mode expansion for piezoelectric plates and certain of its applications*, IEEE Trans. on Ultrasonics, Ferroelectrics and Frequency Control, **35**, 593–611 (1988).
- [24] REKTORIS K., *Variational Methods in Mathematics*, Science and Engineering, Dr. Riedel Publ. Comp., Prague 1980.
- [25] ROCKE C., ZIMMERMANN S., WIXFORTH A., KOTTHAUS J.P., BÖHM G., WEIMANN G., *Acoustically Driven Storage of Light in a Quantum Well*, Phys. Rev. Lett., **78**, 4099–4102 (1997).
- [26] SHIBAYAMA K., YAMANOUCHI K., SATO H., MEGURO T., *Optimum cut for rotated Y-cut LiNbO_3 crystal used as the substrate of acoustic-surface-wave filters*, In Proc. IEEE, **64**, 595–597 (1976).
- [27] SHUYU L., *The three-dimensional equivalent circuit and the natural frequencies of rectangular piezoelectric ceramic resonators*, J. Acoust. Soc. Amer., **96**, 1620–1626 (1994).
- [28] SHUYU L., *Analysis of the sandwich piezoelectric ultrasonic transducer in coupled vibration*, J. Acoust. Soc. Amer., **117**, 653–661 (2005).
- [29] SHUYU L., FUCHENG Z., *Vibrational modes and frequency spectra in piezoelectric ceramic rectangular resonators*, J. Acoust. Soc. Am., **94**, 2481–2484 (1993).
- [30] SMITH R.H., WELSH F.S., *Temperature dependence of the elastic, piezoelectric and dielectric constants of lithium tantalite and lithium niobate*, J. Appl. Phys., **42**, 2219–2230 (1971).
- [31] TIERSTEN H.F., *Hamilton's principle for linear piezoelectric media*, In. Proc. IEEE, 1523, (1967).
- [32] YANG J., *Variational formulation of the equations for small fields superposed on finite biasing fields in an electroelastic body*, IEEE Trans. on Ultrasonics, Ferroelectrics and Frequency Control, **51**, 1030–1034 (2004).